THE JOURNAL OF BIOLOGICAL CHEMISTRY
Vol. 278, No. 39, Issue of September 26, pp. 37122–37131, 2003
Printed in U.S.A.

Distinct Influence of N-terminal Elements on Neuronal Nitric-oxide Synthase Structure and Catalysis*

Received for publication, April 29, 2003, and in revised form, June 25, 2003
Published, JBC Papers in Press, July 7, 2003, DOI 10.1074/jbc.M304456200

Koustubh Panda, Subrata Adak, Kulwant S. Aulak, Jerome Santolini, John F. McDonald, and Dennis J. Stuehr‡

From the Department of Immunology, Lerner Research Institute, Cleveland Clinic, Cleveland, Ohio 44195

Nitric oxide (NO) is a signal molecule produced in animals by three different NO synthases. Of these, only NOS I (neuronal nitric-oxide synthase; nNOS) is expressed as catalytically active N-terminally truncated forms that are missing either an N-terminal leader sequence required for protein-protein interactions or are missing the leader sequence plus three core structural motifs that in other NOS are required for dimer assembly and catalysis. To understand how the N-terminal elements impact nNOS structure-function, we generated, purified, and extensively characterized variants that were missing the N-terminal leader sequence (Δ296nNOS) or missing the leader sequence plus the three core motifs (Δ349nNOS). Eliminating the leader sequence had no impact on nNOS structure or catalysis. In contrast, additional removal of the core elements weakened but did not destroy the dimer interaction, slowed ferric heme reduction and reactivity of a heme-dioxy intermediate, and caused a 10-fold poorer affinity toward substrate L-arginine. This created an nNOS variant with slower and less coupled NO synthesis that is predisposed to generate reactive oxygen species along with NO. Our findings help justify the existence of nNOS N-terminal splice variants and identify specific catalytic changes that create functional differences among them.

Nitric oxide (NO)[1] plays a versatile role in the nervous, immune and cardiovascular systems (1–6). NO is produced by nitric-oxide synthases (NOSs), which catalyze an NADPH-dependent oxidation of L-arginine (Arg) to L-citrulline and NO, with N^{ω}-hydroxy-L-Arg (NOHA) being formed as an enzyme-bound intermediate (7, 8). Three NOS isozymes have evolved to function broadly in mammals: NOS I (neuronal NOS (nNOS)), NOS II (inducible NOS (iNOS)), and NOS III (endothelial NOS (eNOS)). The three NOSs share ~50–60% sequence homology and have closely similar secondary structure (9). Each NOS polypeptide is composed of an N-terminal oxygenase domain that contains iron protoporphyrin IX (heme) and a C-terminal reductase domain that contains FMN, FAD, and an NADPH binding site, with an intervening calmodulin (CaM) binding sequence located between the oxygenase and reductase domains (10, 11). To become active, two NOS polypeptides must form a homodimer (11–14). Dimerization creates an extensive interface between two oxygenase domains, creates high affinity binding sites for (6*R*)-tetrahydrobiopterin (H4B) and Arg in each oxygenase domain, and enables electrons to transfer between NOS flavin and heme groups (15–23).

Expression of nNOS is distinguished by a remarkable diversity. Its gene generates multiple mRNA transcripts through mechanisms including alternative promoter usage, alternative splicing, cassette insertions/deletions, changing sites for 3′-untranslated region cleavage, and polyadenylation as well as allelic diversity in mRNA structure (24, 25). For example, at least nine different exon 1 variants have been identified in the 5′ genomic regions of the human and rat nNOS genes (26–28). These mRNA variants enable expression of a single nNOS protein (wild-type or nNOSα) in a tissue-specific manner (26–28). Of particular interest are the gene expression alterations that produce N-terminally truncated nNOS enzymes, a phenomenon that is not observed among iNOS or eNOS (16, 29, 30). For example, translation initiation within exon 1a gives rise to nNOSβ, which is missing the first 241 N-terminal amino acids (Fig. 1). The missing protein segment represents a N-terminal leader sequence that is unique to nNOS (Fig. 1) and contains PDZ/GLGF structural motifs that help direct nNOS to various protein compartments or complexes within cells (27). nNOSβ has a distinct tissue expression pattern (25), is predominantly located in the cell cytosol, and appears to have near wild-type NO synthesis activity (27). An alternative translation initiation that occurs in exon 5 (Met^{337}) gives rise to nNOSγ, which lacks the first 336 N-terminal amino acids of wild-type nNOS (Fig. 1). The nNOSγ was reported to have low catalytic activity (3% of wild-type) in an *in vitro* assay (27). Curiously, the human testis NOS (TnNOS) that is produced by alternative promoter usage was reported to have significant activity (31), although it is an exact homolog of nNOSγ (Fig. 1). A distinct tissue-specific expression was observed for either variant, implying discreet roles (25).

The TnNOS and nNOSγ enzymes are missing three structural motifs in addition to the N-terminal leader sequence. They represent a β-hairpin hook (termed the N-terminal hook), a C*XXX*C zinc-binding segment, and a segment that binds the 3-hydroxypropyl side chain of H4B (29, 32). These three motifs help form the core oxygenase domain structure that is common in all animal NOS (Fig. 1). Both the N-terminal hook and Zn^{2+} binding motif are thought to be important for stabilizing the NOS dimer. Indeed, the N-terminal hook can swap position with its symmetry mate and thus create a larger dimer inter-

* Supported by National Institutes of Health Grants CA53914 and GM51491 (to D. J. S.). The costs of publication of this article were defrayed in part by the payment of page charges. This article must therefore be hereby marked "*advertisement*" in accordance with 18 U.S.C. Section 1734 solely to indicate this fact.

‡ To whom correspondence should be addressed: Immunology NB3, Lerner Research Institute, Cleveland Clinic, 9500 Euclid Ave., Cleveland, OH 44195. Tel.: 216-445-6950; Fax: 216-444-9329; E-mail: stuehrd@ccf.org.

[1] The abbreviations used are: NO, nitric oxide; NOS, nitric-oxide synthase; nNOS, neuronal nitric-oxide synthase; iNOS, inducible nitric-oxide synthase; eNOS, endothelial NOS; Arg, L-arginine; CaM, calmodulin; H4B, (6*R*)-5,6,7,8-tetrahydro-L-biopterin; EPPS, 4-(2-hydroxyethyl)-1-piperazinepropanesulfonic acid; FL, full-length NOS subunit; OXY, oxygenase subunit; NOHA, N^{ω}-hydroxy-L-Arg; DTT, dithiothreitol; NMDA, *N*-methyl-D-aspartate; TnNOS, human testis NOS.

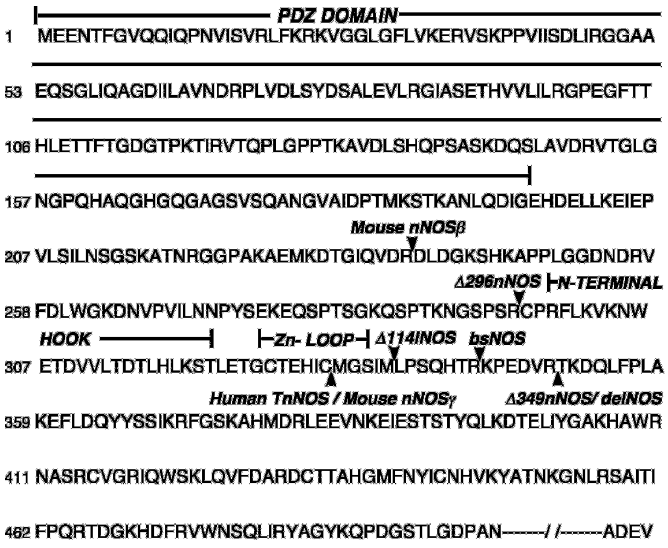

FIG. 1. **The N-terminal protein sequence of rat nNOS (GenBank™ accession number 59949) with the PDZ domain, the N-terminal hook, and the Zn^{2+} binding loop sequences indicated.** The *intervening arrows* indicate the initiation sites for the naturally occurring N-terminal splice variants nNOSβ, nNOSγ, and TnNOS. The *arrows* also indicate the initiation sites of the N-terminally truncated nNOS mutants used in this study (Δ296 and Δ349 nNOS) and the corresponding start sites of an inducible NOS N-terminal deletion mutant (Δ114 mouse iNOS) and NOS-like proteins in genomes of *D. radiodurans* NOS and *B. subtilis* NOS.

face (29, 32), whereas Zn^{2+} binding to the C*XXX*C motif in each subunit covalently links two oxygenase domains (17, 29, 32) .

Because the N-terminal splice variants of nNOS have all been active to varying degrees when overexpressed in animal cells (27, 31), its leader sequence and N-terminal core motifs may not be critical for enzyme assembly and catalysis. Our recent work on bacterial NOS-like proteins from *Deinococcus radiodurans* NOS (33) or *Bacillus subtilis* NOS (34, 35) has shown that they are also catalytically active despite their missing the three core motifs (Fig. 1). Surprisingly, this characteristic of nNOS splice variants and the bacterial NOS-like proteins differs substantially from those of NOS II and NOS III, because in these latter two NOSs the three core motifs are practically essential for dimer formation and associated NO synthesis activity (16, 29, 30). Together, the available data imply that underlying structure-function differences exist among the three NOSs despite their apparent structural congruence. However, little is known about the precise structural requirements of nNOS or why it is the only NOS isoform that is naturally expressed in N-terminally truncated forms.

To explore these issues, we generated, purified, and extensively characterized two N-terminally deleted nNOS proteins, one missing the entire N-terminal leader sequence (Δ296nNOS) and the other missing the leader sequence plus the three core sequence motifs (Δ349nNOS) (29, 32). These particular deletion points represent trypsin-sensitive sites in the otherwise trypsin-resistant nNOS oxygenase domain dimer (nNOSoxy) (36). As shown in Fig. 1, the Δ296nNOS is analogous to the naturally occurring splice variant nNOSβ, whereas the Δ349nNOS is analogous to the naturally occurring nNOSγ and TnNOS splice variants in animals and to the bacterial NOS-like proteins *B. subtilis* NOS and *D. radiodurans* NOS. Our results reveal in detail how the N-terminal structural elements impact nNOS dimer assembly, cofactor/substrate affinity, and several fundamental kinetic and thermodynamic parameters that combine to control its NO synthesis.

MATERIALS AND METHODS

Reagents—All reagents and materials were obtained from Sigma or sources previously reported (29, 37).

Molecular Biology—Restriction digestions, cloning, bacterial growth, transformation, and isolation of DNA fragments were performed using standard procedures. Deletion mutants of full-length rat nNOS, Δ296nNOSFL, and Δ349nNOSFL were constructed by PCR using 5′-end deletion primers incorporating a His_6 tag at the N-terminal end, TTT TTT CAT ATG CAC CAC CAC CAC CAC CAC TGC CCC CGT TTC CTC AAG, for removing residues 1–296 and TTT TTT CAT ATG CAC CAC CAC CAC CAC CAC ACA AAG GAC CAG CTC TTC CC for removing residues 1–349. In both cases, the 3′-end primer GCT TGG CTG AGA ACT TGA CG was used to incorporate a *San*DI unique site in the nNOSFL. PCR products and pCwori plasmid DNA were cut with *Nde*I at the 5′ end and *San*DI at the 3′ end and then ligated at 14 °C overnight. The DNA sequence of all mutants was confirmed by nucleotide sequencing, and the expressed proteins were also checked by N-terminal protein sequencing at the Cleveland Clinic Molecular Biotechnology Core.

Preparation of Wild-type nNOS, nNOSoxy, and Deletion Proteins—Wild-type nNOSFL and the Δ296 and Δ349 mutants contained a His_6 tag attached to their N termini, whereas wild-type nNOSoxy had the His_6 tag attached to its C terminus. All proteins were overexpressed in *Escherichia coli* strain BL21(DE3) using a modified pCwori vector (16). The full-length proteins were purified by sequential chromatography on Ni^{2+}- nitrilotriacetic acid resin and 2′,5′-ADP-Sepharose resin as described previously (38). nNOSoxy was purified by chromatography on Ni^{2+}-nitrilotriacetic acid resin followed by chromatography on Q-Sepharose anion exchange resin (16). The nNOSoxy eluted in the flow-through of the Q-Sepharose column using buffer containing 40 mM EPPS, 10% glycerol, 1 mM DTT, 1 mM Arg, and 0.13 M NaCl. The Δ296nNOSoxy and Δ349nNOSoxy were generated by incubating the above purified nNOSoxy with trypsin (100:1, w/w) for 1 and 11 min, respectively, at 25 °C, following which the reaction was stopped with trypsin inhibitor. Each cleaved nNOSoxy protein was isolated from its reaction mixture by chromatography on Ni^{2+}-nitrilotriacetic acid. The ferrous CO adduct absorbing at 444 nm was used to quantitate heme protein content using an extinction coefficient of 74 mM^{-1} cm^{-1} (A_{444}–A_{500}).

Gel Filtration Chromatography—The purified nNOS proteins (50 μg) were run on a 30 × 10-cm Superdex 200 HR column (Amersham Biosciences) as described before (22).

Arg and H4B Binding—Apparent K_m values for Arg and H4B were derived through double reciprocal analysis of NADPH-dependent NO production rates observed at different concentrations of Arg or H4B at room temperature. Perturbation difference spectrometry was used to determine K_d of Arg according to methods described previously (39).

NO Synthesis, NADPH Oxidation, Ferricyanide Reduction, and Cytochrome c Reduction Activities—Steady state activities of wild-type and mutant nNOS were determined at 25 °C using spectrophotometric assays that were previously described in detail (38), after incubating each purified protein overnight on ice with 5 mM Arg and 10 μM H4B. Activities are reported on the basis of the measured dimer content of each protein. Where calcium-dependent NO synthesis was studied, activities were measured using 0–50 μM calcium chloride in three independent experiments.

H_2O_2-driven NOHA Oxidation—Hydrogen peroxide-driven oxidation of NOHA to nitrite was assayed in 96-well microplates at 37 °C as described previously (22). Final activities were calculated on the basis of the dimeric heme content of each protein.

Kinetics of Enzyme Ferrous Heme-NO Complex Formation during the Initial Phase of NO Synthesis—Enzyme spectral transitions during the initial phase of NO synthesis were studied at 10 °C in the stopped flow spectrophotometer as previously described (40). Reactions were initiated by rapid mixing an air-saturated solution containing 50 μM NADPH with an air-saturated solution containing wild-type or mutant nNOS (2 μM), 40 mM EPPS buffer, pH 7.6, 10 μM H4B, 5 mM Arg, 0.3 mM DTT, 4 μM CaM, and 1 mM Ca^{2+}. Buildup of the enzyme heme-NO complex was monitored at 436 nm. Signal/noise ratios were improved by averaging at least 10 individual mixing experiments. The time courses of absorbance change were best fit to a double exponential equation using a nonlinear least square method provided by the instrument manufacturer.

Heme and Flavin Reduction—The kinetics of heme and flavin reduction were analyzed at 10 °C as described previously (37) using a stopped flow apparatus and diode array detector from Hi-Tech Ltd. (model SF-61) equipped for anaerobic analysis. Ferric heme reduction was

followed by formation of the ferrous CO complex at 444 nm. Reactions were initiated by rapid mixing an anaerobic, buffered, CO-saturated solution containing 50 μM NADPH with an anaerobic, buffered, CO-saturated solution containing wild-type or mutant nNOS (2 μM), 40 mM EPPS buffer, pH 7.6, 10 μM H4B, 5 mM Arg, 0.3 mM DTT, 4 μM CaM, and 1 mM Ca^{2+}. Flavin reduction was monitored under the same conditions at 485 nm. Signal/noise ratios were improved by averaging at least 10 individual mixing experiments. The time course of the absorbance change was fit to single or multiple exponential equations using a nonlinear least square method provided by the instrument manufacturer.

Ferrous Heme-NO Oxidation—An anaerobic buffered solution containing each full-length nNOS enzyme (4 μM) plus 5 mM Arg and 10 μM H4B was reduced with a minimum amount of dithionite solution, and then a saturated NO solution was added to give a NO concentration of ~0.1 mM and form the ferrous heme-NO enzyme complex. This solution was transferred to the stopped flow under anaerobic conditions and then rapidly mixed with air-saturated buffer solution at 10 °C. Rates of ferrous NO complex disappearance and ferric enzyme formation were determined from cross-sections of absorbance loss and gain at 436 and 393 nm, respectively.

Single Turnover Analysis of Arg or NOHA Oxidation—These reactions were performed as previously described (41). An anaerobic solution of nNOSoxy enzyme (6 μM) containing 40 mM EPPS, pH 7.6, 1 mM DTT, and 2 mM NOHA or 5 mM Arg, with or without 20 μM H4B, was titrated with dithionite solution in an anaerobic cuvette until full reduction to ferrous nNOSoxy was achieved. The solution was then transferred to the stopped flow instrument using a gas-tight syringe, where it was rapidly mixed in multiple shots with an equal volume of oxygen-saturated buffer (50 mM EPPS, pH 7.6) at 10 °C. Ninety-six spectral scans (330–700 nm) were obtained following each mixing. The diode array data were then fit to different reaction models by a Specfit program from Hi-Tech Ltd. to obtain the calculated number of species, their individual spectra, the concentration of each species *versus* time, and rate constants for each transition.

Measurement of Heme Midpoint Potential—The glass cell and electrodes used were as previously described (42). Spectroelectrochemical titration was performed at 25 °C using a Radiometer PGP201 potentiostat/galvanostat. The reference and auxiliary electrodes were made anaerobic overnight in a solution containing 0.5 mM methyl viologen, 0.1 M potassium phosphate, pH 7. The reference electrode was calibrated using a 5 mM solution of ferricyanide/ferrocyanide in anaerobic 0.1 M potassium phosphate, pH 7, at 25 °C (E_m = +425 mV). The Δ296nNOSoxy and Δ349nNOSoxy were diluted to a final concentration of about 25 μM in a 0.1 M potassium phosphate buffer, pH 7, in the presence of 60 μM H4B, 0.1 mM EDTA, 5 mM Arg, 0.1 mM methyl viologen, 20 μM phenosafranine, and 20 μM neutral red. The solution was rendered anaerobic in the electrochemical cell by N_2 refilling over 2 h. The titration was achieved using the internal source of the radiometer set on the galvanostat mode for current ranging between 5 and 60 μA and times ranging between 15 s and 5 min. After each adjustment, the potential was allowed to equilibrate (between 30 min and 1 h), the potential was measured (*versus* SHE), and a spectrum was recorded on a Hitachi U-3110 spectrophotometer. The one-electron midpoint potential was determined using the absorbance change at 400 and 645 nm, where change due to dye mediators was negligible. The midpoint potential was calculated using the Nernst equation.

RESULTS

Physical Characteristics of N-terminal Deletion Mutants—The full-length proteins Δ296nNOSFL and Δ349nNOSFL were generated by deletion mutagenesis, whereas corresponding nNOSoxy proteins were generated by limited trypsin proteolysis of purified nNOSoxy (43). Fig. 2 depicts SDS-PAGE and gel filtration profiles of the six proteins used in our study, namely wild-type nNOSoxy (*A*), Δ296nNOSoxy (*B*), Δ349nNOSoxy (*C*), wild-type nNOSFL (*D*), Δ296nNOSFL (*E*), and Δ349nNOSFL (*F*). Each protein migrated at its expected molecular weight in SDS-PAGE. N-terminal sequencing confirmed that each protein had the correct N-terminal truncation (data not shown). Gel filtration patterns showed that N-terminal deletions of 296 or 349 amino acids did not greatly alter the dimer content of the nNOSoxy proteins, given that even Δ349nNOSoxy remained 83% dimeric (Fig. 2, *panel 2*, *profile C*). The full-length proteins, however, had generally less dimer content compared

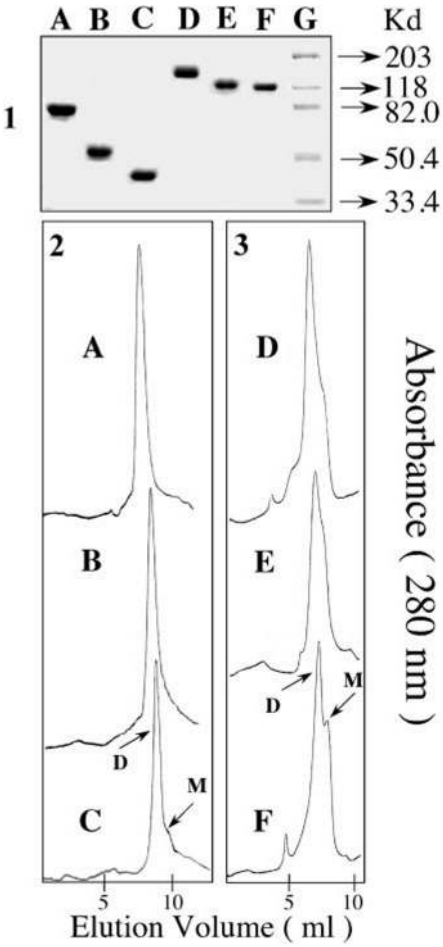

FIG. 2. **SDS-PAGE (*panel 1*) and gel filtration profiles (*panels 2 and 3*) of wild-type and N-terminally deleted nNOS proteins.** 10–15 μg of each protein (*A*, wild-type nNOSoxy; *B*, Δ296nNOSoxy; *C*, Δ349nNOSoxy; *D*, wild-type nNOSFL; *E*, Δ296nNOSFL; *F*, Δ349nNOSFL) were analyzed by gel electrophoresis after being boiled in the presence of 10% SDS and β-mercaptoethanol. *Lane G* (*panel 1*) shows the protein molecular weight standards. The corresponding gel filtration patterns are for the oxygenase domain (*panel 2*) and full-length enzymes (*panel 3*) run on a Superdex 200 HR column as described under "Materials and Methods." Results are representative of three similar experiments. *D*, dimer; *M*, monomer.

with their oxygenase counterparts, consistent with our earlier observations that attached reductase domains weaken the dimeric interaction between two oxygenase domains (44). Thus, nNOSFL, Δ296nNOSFL, and Δ349nNOSFL were estimated to be 88, 82, and 56% dimeric, respectively (Fig. 2, *panel 3*). Notably, the truncated nNOSFL proteins did not increase their dimer content after overnight incubation with 10 mM Arg and 20 μM H4B (data not shown) as otherwise normally occurs in wild type enzyme (13 ,43). Our results suggest that the N-terminal leader sequence and adjacent core elements need not be present for significant dimer formation in nNOS. This behavior makes nNOSoxy somewhat similar to bacterial NOS-like proteins (33–35) and distinguishes them from the other two mammalian isoforms, iNOS or eNOS, where deletion of the same core elements renders them completely or predominantly monomeric (16, 29, 30).

Because a significant proportion of each N-terminal-deleted nNOS was dimeric, the nNOSs provided us an unprecedented opportunity to investigate how the N-terminal elements influence kinetic, thermodynamic, and catalytic properties of a nNOS dimer. These investigations are detailed below.

Role of N-terminal Elements in Stabilizing the Dimer—We compared dimer interaction strengths of the various full-length

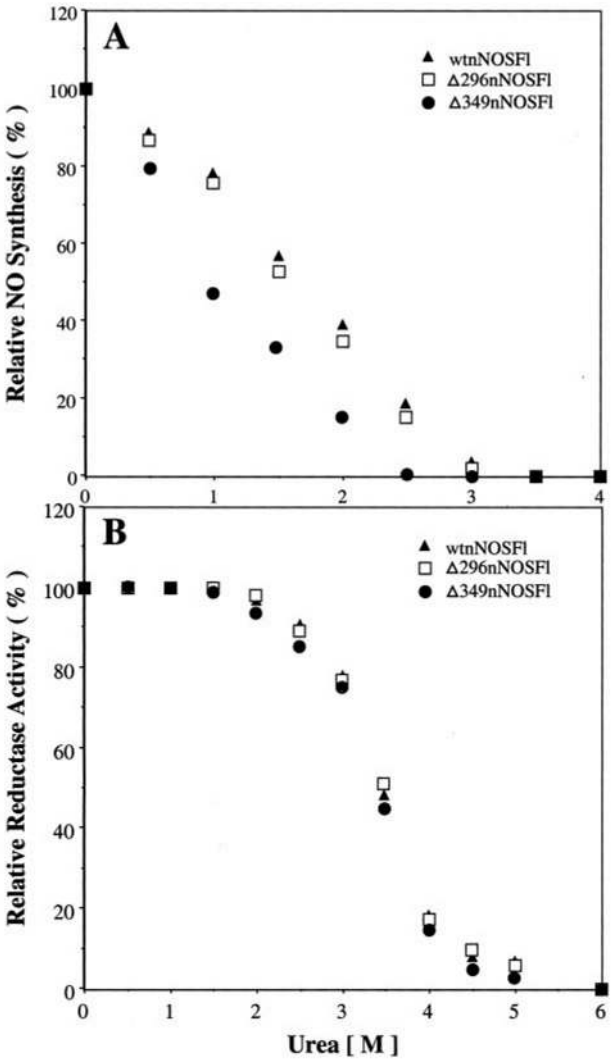

FIG. 3. **Catalytic activities of nNOS full-length proteins after incubation with increasing concentrations of urea.** Enzymes purified in the absence of Arg and H4B were incubated at 15 °C with the indicated concentrations of urea for 2.5 h. Sample aliquots were then diluted about 10 times and assayed for NO synthesis (*A*) or cytochrome *c* reduction (*B*) as described under "Materials and Methods." Data are representative of three similar experiments.

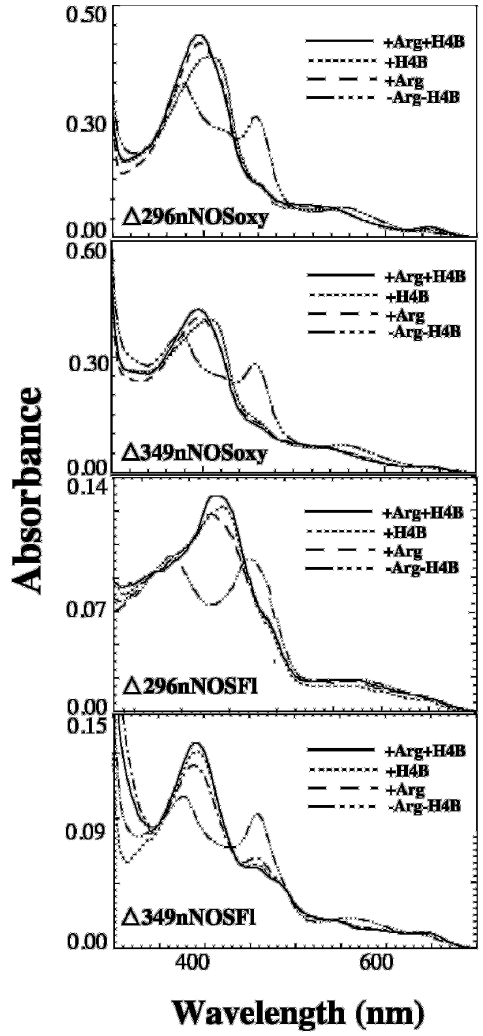

FIG. 4. **Light absorption spectra of nNOS proteins in the presence and absence of H4B and Arg.** Spectra were recorded at 25 °C in buffer containing 2 mM DTT alone or after incubating proteins overnight at 4 °C in buffer containing DTT and 10 mM Arg and/or 20 μM H4B.

proteins by examining the loss of a dimer-dependent and a dimer-independent catalytic activity as a function of increasing chaotropic stress due to urea (43). Fig. 3*A* shows that Δ349nNOSFL lost dimer-dependent activity (NO synthesis) at lower urea concentrations compared with wild type nNOSFL or to Δ296nNOSFL. However, the three proteins were identical regarding stability of their dimer-independent activity (cytochrome *c* reduction; Fig. 3*B*). This indicates that the N-terminal leader sequence has no impact on nNOS dimer stability, whereas the three core structural elements do. However, significant dimer stability remains even in their absence.

Spectral Properties and Arg and H4B Affinity—Dithionite reduction of each nNOS mutant in the presence of CO formed a ferrous heme-CO complex that absorbed at 444 nm in all cases (not shown), indicating that they all have proper heme incorporation with stable cysteine thiolate axial ligation (44). Light absorbance spectra of the four ferric proteins are shown in Fig. 4. In the presence of 1 mM DTT, all proteins exhibited a split Soret absorbance peak at 380 and 460 nm, which indicated that DTT bound to ferric heme to form a bis-thiolate complex as occurs in wild-type nNOS (22). Arg and H4B were able to displace DTT and bind to all four mutants, as indicated by a characteristic shift in Soret absorbance toward a single peak near 400 nm (45, 46).

Arg binding affinities were determined by measuring displacement of imidazole bound to the ferric heme at different Arg concentrations (22, 39). The Δ349nNOSFL had almost 10-fold higher apparent K_d for Arg compared with wild type, whereas the apparent K_d of Δ296 nNOSFL was equivalent to wild type (Table I). Measures of the apparent K_m for Arg using the NO synthesis assay also showed a higher value for the Δ349nNOSFL (Table I). Measures of apparent K_m for H4B indicated a less than 2-fold increase for Δ349 nNOSFL compared with wild type (Table I). These data suggest that the N-terminal leader sequence has no impact on Arg or H4B binding affinity or K_m, whereas an additional deletion of the core elements lowers enzyme affinity toward Arg and H4B and increases their apparent K_m.

NOS Steady State Catalytic Activities—We compared catalytic activities of the three nNOS proteins by measuring their steady state rates of NO production and associated NADPH oxidation, H_2O_2-dependent nitrite formation from NOHA, and cytochrome *c* and ferricyanide reduction (38). Results are summarized in Tables II and III. After taking into account their differences in dimer content, NO synthesis activity of

Δ296nNOSFL was 93% of the wild type nNOSFL, whereas Δ349nNOSFL had 45% activity of wild type (Table III). Corresponding NADPH oxidation rates measured during NO synthesis showed that the ratio of NADPH oxidized per NO formed was similar in the Δ296nNOSFL and wild type enzymes (2.2 and 2.0, respectively) but was a bit greater in Δ349nNOSFL (2.6) (Table III). The rates of nitrite production by Δ296nNOS and Δ349nNOS in the H_2O_2-driven assay were 91 and 51% that of wild type, respectively, and were in consonance with their NO synthesis activities (Table II). All three enzymes had equivalent cytochrome *c* and ferricyanide reductase activities.

We also examined whether there was any change in the Ca^{2+} dependence of the Δ349nNOSFL as compared with the wild type. We found that both proteins showed a similar trend of Ca^{2+}-dependence over a 0–50 μM concentration range (data not shown), indicating that the deletion of 349 amino acids from the N-terminal region did not affect Ca^{2+} response in nNOS.

Together, these data suggest that deleting the N-terminal leader sequence had no impact on catalysis, whereas removal of the three N-terminal core elements slowed NO synthesis by the nNOS dimer and caused some uncoupling of its NADPH oxidation. To better understand the basis for these catalytic effects, we performed kinetic and biophysical studies with the nNOS deletion mutants as described below.

Kinetics of Heme and Flavin Reduction—We determined the kinetics of NADPH-dependent flavin and heme reduction in CaM-bound nNOS proteins by stopped flow spectroscopy. The observed rate constants for reactions run at 10 °C are listed in Table IV, and the traces in Fig. 5 illustrate kinetics of absorbance change recorded at two diagnostic wavelengths for each nNOSFL protein (37).

Rates of NADPH-dependent flavin reduction were strikingly close in all three proteins (Fig. 5*B*), confirming that the N-terminal elements do not influence electron loading into the reductase domain. We determined the kinetics of heme reduction by following heme CO binding at 444 nm (47). The initial absorbance decrease present in each trace of Fig. 5*B* reflects an NADPH-dependent flavin reduction that occurs prior to electron transfer to the ferric heme (38) and was not considered in our rate calculations. Heme reduction was best described as monophasic in all three proteins (Fig. 5*A*). The Δ296nNOSFL and wild type enzymes were equivalent regarding their rates and extents of heme reduction. In contrast, heme reduction in Δ349nNOSFL was 27% slower and of smaller magnitude than wild type (Table IV). The smaller magnitude for Δ349nNOSFL heme reduction is likely to be due to the lower dimer content of this mutant. Control reactions showed that rates of CO binding by the prereduced ferrous forms of all three nNOS proteins were identical (data not shown), confirming that the differences we observed reflected their different ferric heme reduction rates. Removal of the core N-terminal elements, therefore, caused a discernible slowing of ferric heme reduction in Δ349nNOSFL.

Heme-NO Complex Formation and Oxidation—We next compared rates of heme-NO complex buildup during the initial phase of NO synthesis by the three nNOSFL enzymes (47). Heme-NO complex formation was followed at 436 nm after initiating NO synthesis with NADPH addition in the stopped flow instrument. Complex buildup occurred within the first few seconds and followed a biphasic process in all cases, with the slow phase representing the majority of the total absorbance change (Table IV). The relative rates of heme-NO complex buildup were as follows: wild type = Δ296nNOSFL > Δ349nNOSFL. This matched the rank order of their ferric heme reduction rates and is consistent with ferric heme reduction being rate-limiting for heme-NO complex formation in the initial phase of NO synthesis.

During steady state NO synthesis, a significant proportion of nNOS builds up as a ferrous heme-NO complex, and oxidation of this complex to ferric enzyme is one of three kinetic parameters that together determine the release rate of NO (48). We therefore investigated whether the N-terminal deletions would affect the rate of ferrous heme-NO oxidation. All three nNOSoxy enzymes formed stable six-coordinate ferrous heme-NO complexes in the presence of Arg and H4B (data not shown). Their rates of oxidation to form ferric enzyme were similar (Table IV). This suggests that the N-terminal deletions do not alter the oxygen reactivity of the nNOS ferrous heme-NO complex.

Single Turnover Reaction Kinetics—To investigate whether the N-terminal deletions affect any of the defined biosynthetic steps that occur during a single catalytic turnover by nNOS

TABLE I
Arg and H4B interaction

Apparent K_m values were derived from NO synthesis measurements taken at room temperature. K_d for Arg was determined using perturbation difference spectroscopy. Results shown are the mean and S.D. of three independent experiments. WT, wild-type.

Protein	Arg		H4B K_m
	K_d	K_m	
	μM		μM
WT nNOSFL	4.2 ± 0.3	4.8 ± 0.2	0.50 ± 0.03
Δ296nNOSFL	4.7 ± 0.2	5.4 ± 0.3	0.54 ± 0.03
Δ349nNOSFL	57.1 ± 3.4	68.5 ± 4.4	0.82 ± 0.05

TABLE II
H_2O_2-dependent NOHA conversion to nitrite

Reactions were run at 37 °C and stopped after 10 min by the addition of 1300 units of catalase. Values are the mean and S.D. from three independent experiments. WT, wild-type.

Protein	Activity
	mol nitrite formed/mol dimer heme/min
WT nNOSoxy	18.5 ± 1.1
Δ296nNOSoxy	16.7 ± 0.9
Δ349nNOSoxy	9.4 ± 0.4
WT nNOSFL	16.4 ± 0.8
Δ296nNOSFL	14.9 ± 0.5
Δ349nNOSFL	8.7 ± 0.2

TABLE III
Steady state catalytic activities

Rates were measured at 25 °C. NO synthesis from Arg and concurrent NADPH oxidation were measured under identical assay conditions. Other activity assays are described under "Materials and Methods." Turnover number is expressed as moles of product formed/moles of dimer heme/min. Values represent the mean ± S.D. of three independent measurements. WT, wild-type.

Enzyme	NO synthesis		NADPH oxidation	Cytochrome c reduction		Ferricyanide reduction	
	+CaM	−CaM	+CaM	+CaM	−CaM	+CaM	−CaM
	min^{-1}		min^{-1}	min^{-1}		min^{-1}	
WT nNOSFL	64.6 ± 0.5	Nil	127.9 ± 3.8	5742 ± 116	462 ± 11	5182 ± 300	955 ± 32
Δ296nNOSFL	60.1 ± 1.9	Nil	135.4 ± 3.3	5720 ± 213	447 ± 36	5159 ± 254	949 ± 56
Δ349nNOSFL	28.8 ± 1.1	Nil	75.2 ± 0.2	5701 ± 241	422 ± 27	5156 ± 300	930 ± 26

TABLE IV

Rates of heme reduction, flavin reduction, ferrous heme-NO buildup, and ferrous heme-NO oxidation

All reactions were run at 10 °C in a stopped-flow spectrophotometer. Rates of flavin and heme reduction were obtained for CaM-bound enzymes in reactions triggered by NADPH addition in the presence of CO. Rates of enzyme heme-NO complex buildup were recorded during the initial phase of NO synthesis. Rates of ferrous heme-NO complex oxidation were obtained by reacting anaerobic ferrous-NO enzymes with an air-saturated solution. Values in parenthesis indicate the rate of ferric enzyme formation as determined at a separate wavelength in the same oxidation reactions. Details are described under "Materials and Methods." The values are representative of eight separate reactions for each experiment. WT, wild-type.

Enzyme	Heme reduction (k)	Flavin reduction		Heme-NO complex buildup		Ferrous heme-NO oxidation (k)
		k_1	k_2	k_1	k_2	
	s^{-1}	s^{-1}		s^{-1}		s^{-1}
Wt nNOSFL	4.6 ± 0.2	48.3 ± 1.8	4.2 ± 0.3	9.4 ± 0.7	2.0 ± 0.08	0.17 ± 0.08 (0.16 ± 0.06)
Δ296nNOSFL	4.6 ± 0.3	47.4 ± 2.6	4.6 ± 0.2	9.1 ± 0.6	2.0 ± 0.02	0.16 ± 0.02 (0.16 ± 0.03)
Δ349nNOSFL	3.4 ± 0.1	47.2 ± 3.1	4.1 ± 0.3	7.0 ± 0.2	0.8 ± 0.03	0.14 ± 0.03 (0.13 ± 0.04)

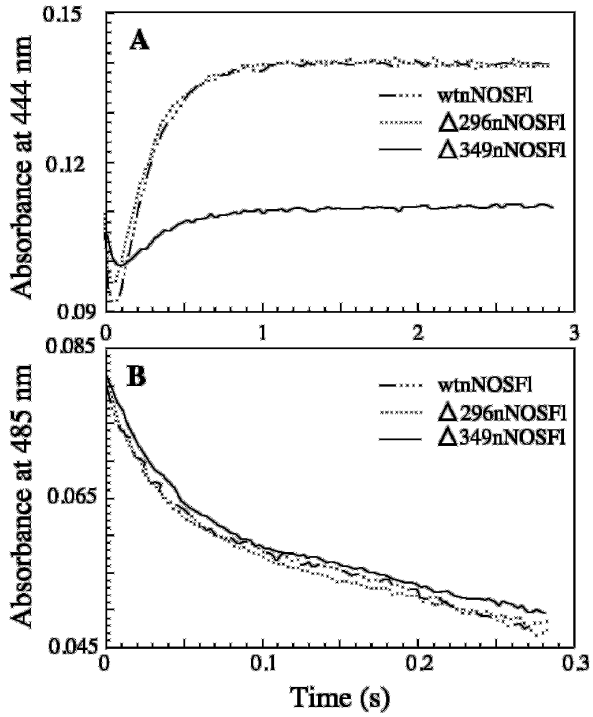

FIG. 5. **Kinetics of heme and flavin reduction in the nNOS enzymes at 10 °C.** Reactions were initiated by mixing CaM-bound enzymes with NADPH under anaerobic conditions in the stopped flow spectrophotometer. Heme reduction (*A*) was followed by CO binding at 444 nm, whereas flavin reduction (*B*) was followed at 485 nm. Traces shown are the average of 7–10 individual scans.

(41, 49), we utilized rapid scanning stopped flow spectroscopy to monitor the consecutive heme transitions that occur during Arg or NOHA oxidation in a single turnover reaction. All reactions were done at 10 °C and were initiated by rapidly mixing an oxygen-containing buffer with a prereduced ferrous nNOSoxy protein that contained 5 mM Arg or 2 mM NOHA and 20 μM H4B (except when indicated).

In all three nNOSoxy proteins, we discerned formation of an initial ferrous-dioxy intermediate and its subsequent conversion to ending ferric enzyme, as previously reported for the Arg reaction of wild-type nNOSoxy (41). The spectral properties of the ferrous-dioxy intermediates were identical. However, the rates at which the ferrous-dioxy intermediate converted to ferric enzyme in the Δ296nNOSoxy and Δ349nNOSoxy Arg reactions were 72 and 45% as fast as in the wild type reaction, respectively (Table V). This indicated that the N-terminal deletions could slow down this particular catalytic transition.

Analysis of rapid scan data collected during the NOHA single turnover reactions discerned formation of the initial ferrous-dioxy intermediate, an initial ferric heme-NO product complex, and the ending ferric enzyme for all three nNOSoxy proteins (Fig. 6). Each spectral species had characteristic absorbance bands that have been previously observed for wild-type nNOSoxy (41). The three nNOSoxy proteins had similar rates for each of the three catalytic transitions that are observed during the NOHA reaction (Table V). This indicated that the N-terminal deletions do not impact the kinetics of NOHA oxidation or subsequent dissociation of NO from the ferric enzyme.

Heme Midpoint Potential—We also examined whether the N-terminal deletions changed the nNOS ferric heme midpoint potential. Fig. 7, *upper left panel*, shows light absorbance spectra collected during electrochemical titration of Δ296nNOSoxy. Absorbance change at 400 and 645 nm was used to calculate reduction potential, because at those wavelengths the spectral change due to the added mediator dyes is negligible. The *lower left panel* shows the Nernst plot for the absorbance data at 645 nm for Δ296nNOSoxy. The slope obtained was 0.046 (for 0.059), and the midpoint potential was calculated to be −260 ± 8 mV. The *upper right panel* of Fig. 7 contains spectra collected during titration of Δ349nNOSoxy, whereas the *lower right panel* shows the Nernst plot of the absorbance data collected at 650 nm. The calculated heme midpoint potential for Δ349nNOSoxy was −273 mV ± 5 mV, with a slope of 0.062. These midpoint values are comparable with a wild type heme midpoint potential of −257 mV ± 3 mV.

DISCUSSION

The normal dimer content, urea resistance, and catalytic profile of our Δ296nNOS enzymes establish that the N-terminal leader sequence has practically no role in dimer stability or enzyme catalysis. Our results with Δ296nNOS confirm and extend previous work that had demonstrated that mouse nNOS lacking the PDZ domain (nNOSβ), which is analogous to a Δ241nNOSFL, retained about 80% of the wild-type nNOS activity when transfected into COS cells, with the activity being fully dependent on Ca^{2+}/CaM and displaying a normal K_m for Arg (27). It is now clear that except for providing binding sites for protein inhibitor or stimulator molecules like PIN (protein inhibitor of nNOS), the NMDA receptor, or CAPON (carboxyl terminal PDZ ligand of nNOS) (50–52), the nNOS leader sequence is not meant to discharge any structural or catalytic functions to the enzyme. Rather, its role is to direct nNOS toward various protein-protein interactions that help regulate NO production and signal transduction (53). In neuronal tissues, for example, nNOS enzymatic activity is dependent on calcium influx through NMDA receptors, and this may require

TABLE V

Kinetics of heme transitions during Arg and NOHA single turnover reactions

Anaerobic ferrous nNOSoxy proteins that contained Arg or NOHA in the presence or absence of H4B were rapidly mixed at 10 °C in the stopped flow spectrophotometer with oxygen-saturated buffer to start the reactions. Heme transitions were examined by rapid scanning spectroscopy. Values are means ± S.D. for between 8 and 15 individual reactions per experiment. k_1, k_2, k_2', and k_3 are the conversion rates for the transitions indicated in Reactions 1 and 2, the single turnover reactions of Arg and NOHA, respectively. WT, wild-type.

$$\text{FeII-Arg} + O_2 \xrightarrow{k_1} \text{FeIIO}_2\text{-Arg} \xrightarrow{k_2} \text{FeIII} + \text{NOHA}$$

REACTION 1

$$\text{FeII-NOHA} + O_2 \xrightarrow{k_1} \text{FeIIO}_2\text{-NOHA} \xrightarrow{k_2'} \text{FeIII NO} + \text{citrulline} \xrightarrow{k_3} \text{FeIII} + \text{NO}$$

REACTION 2

Reaction	Heme-dioxygen buildup (k_1)	Heme-dioxygen disappearance		Ferric heme-NO decay (k_3)
		k_2	k_2'	
	s^{-1}	s^{-1}		s^{-1}
WT nNOSoxy + Arg + H4B	138 ± 8.2	18 ± 0.8		
WT nNOSoxy + Arg	121 ± 6.4	0.3 ± 0.05		
WT nNOSoxy + NOHA + H4B	129 ± 4.7		29 ± 1.1	5 ± 0.6
Δ296nNOSoxy + Arg + H4B	118 ± 5.8	13 ± 0.6		
Δ296nNOSoxy + Arg	106 ± 8.3	0.4 ± 0.02		
Δ296nNOSoxy + NOHA + H4B	146 ± 3.1		26 ± 0.7	5 ± 0.3
Δ349nNOSoxy + Arg + H4B	122 ± 5.5	8.2 ± 0.4		
Δ349nNOSoxy + Arg	93 ± 6.7	0.1 ± 0.02		
Δ349nNOSoxy + NOHA + H4B	90 ± 7.2		23 ± 0.4	4.4 ± 0.2

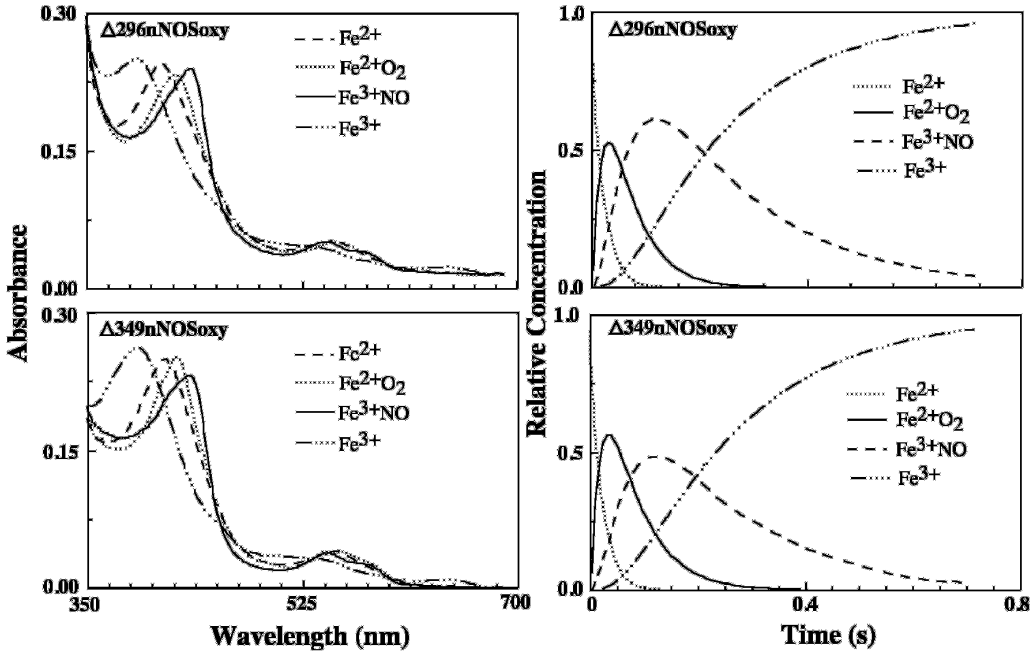

FIG. 6. **Light absorption spectra of four heme species identified during NOHA single turnover reactions (*left panels*) and their changes in concentration *versus* time (*right panels*).** Anaerobic solutions of ferrous NOSoxy proteins (Δ296 and Δ349) containing NOHA (2 mM) and H4B (20 μM) were mixed with air-saturated buffer at 10 °C in the stopped flow instrument, and diode array spectra were collected. *Traces* in each *panel* are the averages from 8–10 reactions each.

the nNOS to be attached to the NMDA receptor through the PDZ/GLGF domain located in the leader sequence (54). This localization might also be important for nitration of the NMDA receptor and its functional consequences (55). In skeletal muscles, nNOS is similarly localized through its PDZ/GLGF interaction with syntrophin, which in turn associates nNOS with the dystrophin complex that is anchored to the sarcolemma (27, 56). Variants like nNOSβ or our Δ296nNOS would thus lack proper localization for a precise regulation or delivery of NO in skeletal muscle tissues (27).

The N-terminal core elements of NOS consist of the N-terminal hook, a C*XXX*C Zn^{2+} binding motif, and a segment of residues that interact with the dihydroxypropyl side chain of H4B (Fig. 1). Deleting the three elements in mouse iNOS led to a completely monomeric, thiol-ligated heme protein that was catalytically inactive and unable to bind Arg or H4B (16, 29, 30). A similar deletion in bovine eNOS (analogous to the first 115 amino acids in iNOS) generated an enzyme that was predominantly monomeric and retained little catalytic activity (16, 29, 30). In contrast, our Δ349nNOSFL and Δ349nNOSoxy proteins were 56 and 83% dimeric and maintained substantial catalytic activity. Thus, among the three mammalian NOS, only nNOS withstands such an extensive deletion.

Our previous work showed that dimer interaction strengths

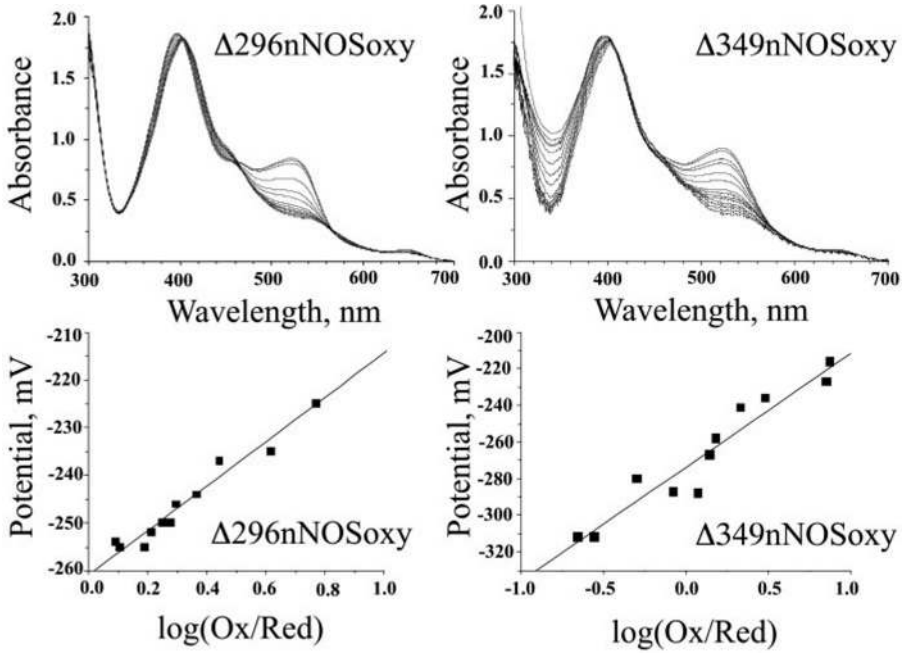

FIG. 7. **Heme midpoint potentials of the Δ296 and Δ349 nNOSoxy mutants.** The *upper panels* contain light absorbance scans taken during the reductive titrations. Reduction was achieved using an internal electron source and three different redox mediators as described under "Materials and Methods." The *lower panels* show the Nernst plots derived from absorbance changes at 650 nm. Data were fit to a line using Origin 5.0© and are representative of two titrations.

follow a rank order of eNOS > nNOS > iNOS (43). However, after deletion of the three core N-terminal elements, the rank order changes to nNOS > eNOS > iNOS. Thus, although the three core elements still help to stabilize the nNOS dimer (see Figs. 2 and 3), their contributions are less critical for nNOS than for iNOS or eNOS. This implies that nNOS depends more on interactions within the remaining dimer interface. The mechanisms by which N-terminal core elements may stabilize NOS dimers include exchange of N-terminal hooks between the two oxygenase domains in the dimer (29, 32) and Zn^{2+} ligation of four cysteines located at the dimer interface (17, 32). Curiously, mutation of two conserved residues in the N-terminal hook of nNOS (Asp-314 and Thr-315) decreased dimer stability and catalysis to a greater extent than did our Δ349 deletion (57). Although surprising, this relationship is consistent with our finding that analogous point mutations in the iNOS N-terminal hook antagonize heterodimer formation to a greater extent than does complete deletion of the N-terminal core elements (16, 29, 30). Although Zn^{2+} binding has been shown to help to stabilize the nNOS dimer against dissociation in polyacrylamide gels (58), our results clearly indicate that an intact $Zn^{2+}(Cys)_4$ site is not required for significant nNOS dimerization or for its catalytic function. This conclusion is consistent with point mutagenesis studies that showed an intact $Zn^{2+}(Cys)_4$ complex is not required for the dimerization or activity of nNOS or iNOS (29, 59, 60).

Our current findings help justify the existence of biologically active nNOS splice variants like human TnNOS and the mouse nNOSγ (27, 31) and also justify how NOS-like proteins present in *D. radiodurans* NOS or *B. subtilis* NOS can be dimeric and catalytically active despite their missing all three N-terminal core elements (33–35). In fact, our Δ349nNOSoxy construct is exactly analogous to *D. radiodurans* NOS (Fig. 1). The *D. radiodurans* NOS and *B. subtilis* NOS enzymes were shown to produce either NO or nitrite when combined with a mammalian NOS subunit in a heterodimer, when supported by a free mammalian NOS reductase domain (33), or in a single turnover reaction using NOHA as substrate (34). Together, such evidence provides new perspective on the selective importance of the N-terminal core elements in NOS dimerization and function.

The NO synthesis activity of the Δ349nNOSFL dimer was only 45% compared with wild type enzyme. There are three key kinetic parameters that together determine the NO release rate from a given NOS during its steady state catalysis (48). These are the rate of ferric heme reduction, the rate of ferric heme-NO complex dissociation, and the rate of ferrous heme-NO oxidation. We found that the rate of ferric heme reduction was slower in Δ349nNOSFL compared with wild type, whereas the two other key kinetic parameters were only slightly altered. A slowing of nNOS ferric heme reduction has been accomplished using CaM mutants (37, 61). In that circumstance, a slower rate of ferric heme reduction in nNOS was associated with a proportionally slower NO synthesis in the steady state. Computer simulation using a kinetic model that describes nNOS catalysis also predicted this same result (62). We therefore can conclude that the slower NO synthesis by the Δ349nNOSFL dimer is primarily due to its slower rate of ferric heme reduction, as measured directly in our stopped flow experiments.

How might the Δ349 deletion slow down heme reduction in nNOS? One mechanism could involve changing the thermodynamic driving force for heme reduction, as occurs in Trp^{409} point mutants of nNOS (63, 64). However, we know this is not the case for Δ349nNOS, because its heme midpoint potential is similar to that of wild type. Alternatively, the N-terminal core elements may help to properly align or gate the FMN module in its contacting the oxygenase domain for ferric heme reduction. This role would be consistent with NOSoxy crystal structures that show the deleted N-terminal elements are adjacent to a region on the oxygenase domain surface that is predicted to help dock the FMN module for electron transfer to the heme (32, 35). Our previous work with iNOS N-terminal deletion mutants showed that their NO synthesis is also slower than wild type when tested in a heterodimer system (29). This possibly reflects a slower heme reduction, but further study will be required.

Why does the Δ349 deletion not affect rates of nNOS ferric heme-NO dissociation or ferrous heme-NO oxidation? In the former case, crystal structures show that the deleted N-terminal elements are located near the open end of the active site funnel (32) and so are probably too far away from the heme pocket to influence heme-NO dissociation. In the latter case, a lack of effect is consistent with this deletion not altering the

nNOS heme midpoint potential, which otherwise affects the rate of ferrous heme-NO oxidation,[2] and with its not causing any discernible change in the heme electronic environment.

Together, our analysis of the three key kinetic parameters predicts that Δ296nNOSFL and Δ349nNOSFL enzyme molecules will distribute themselves during steady state NO synthesis in much the same way as does wild type nNOS (*i.e.* the predominant enzyme species will be the ferrous heme-NO complex) (48). This means that both deletion mutants should preserve the high apparent K_{m,O_2} that is characteristic of wild type enzyme (K_{m,O_2} of ~0.4 mM) (65). Thus, biological expression of such N-terminal splice variants is not likely to provide a nNOS with a modified physiologic oxygen response.

In addition to its poor dimerization and slower NO synthesis, two features that distinguish Δ349 nNOSFL are its less coupled NADPH oxidation and NO synthesis and a 10-fold poorer Arg binding affinity. The uncoupled NADPH oxidation may be biologically important, because the active enzyme will produce reduced oxygen species along with NO. Different factors may contribute to the greater uncoupling in Δ349 nNOSFL. For example, it could be due to problems with subdomain alignment as discussed above in the context of ferric heme reduction. Another causative factor may be the slower reaction of the ferrous-dioxy intermediate during Arg hydroxylation. The speed of this conversion is directly linked to the efficiency of Arg hydroxylation, and slowing this step is one way to uncouple NADPH oxidation and NO synthesis (66). Because the rate of ferrous-dioxy conversion is determined by the rate of H4B electron transfer in NOS (66), our results imply that H4B radical formation might be slower in Δ349nNOS. Interestingly, conversion of the ferrous-dioxy species is also slower in *D. radiodurans* NOS and *B. subtilis* NOS (33, 34), which are also missing the N-terminal core elements. How the N-terminal core elements influence the rate of ferrous-dioxy conversion is an important structure-function question that will require further study.

Regarding the poorer Arg binding affinity of Δ349nNOS, the same effect was observed for N-terminal deletion mutants of eNOS (30) and for a nNOS point mutant C331A, whose Zn^{2+} binding is selectively disrupted (67). However, poor Arg binding was not observed for iNOS point mutant C109A, whose Zn^{2+} binding is also selectively disrupted in the same way (29). Arg binding affinity is also normal in *D. radiodurans* NOS and *B. subtilis* NOS (33, 34) despite their missing the three N-terminal core elements. Thus, the influence of N-terminal core elements on Arg binding in NOS is isoform-specific. The poorer Arg affinity in Δ349nNOS is probably biologically significant, because it would increase by a factor of 10 the intracellular Arg concentration required to maintain saturation binding for coupled NO synthesis.

It is also noteworthy that Δ349nNOSFL displayed little change in its K_m for H4B. This same behavior was observed in the presence of Arg for an nNOS mutant with a disrupted Zn^{2+} binding site (67) and for N-terminal deletion mutants of eNOS (30). Similarly, point mutation of core N-terminal residues that interact with the dihydoxypropyl side chain of H4B had no significant effect on H4B affinity of iNOSoxy (29). Recently, *B. subtilis* NOS was also shown to have normal H4B affinity despite its missing the N-terminal core elements (34). On the other hand, an iNOSoxy whose Zn^{2+} center was disrupted by point mutagenesis had about a 7-fold poorer affinity toward H4B (29), and differences observed in crystal structures of Zn^{2+}-free and Zn^{2+}-bound iNOSoxy dimer led to the conclusion that the Zn^{2+} center should strongly influence the energetics of H4B binding in iNOS (68). Taken together, these data argue that N-terminal core elements play relatively minor roles in regulating H4B binding to nNOS, eNOS, and possibly even iNOS. Indeed, key residues that surround the H4B ring and position it near the heme are conserved in all bacterial NOS-like proteins (35, 69) and remain present in all of the N-terminal deletion mutants discussed above. Individual mutation of these residues typically does lower NOS affinity toward H4B (29). A concept that does emerge from the NOS mutational studies is that maintaining a dimeric structure correlates well with maintaining a capacity to bind H4B. On the other hand, there is no such correlation between maintaining dimeric structure and a capacity to bind Arg (22, 39, 70). This may reflect that the H4B binding sites are integrated into the NOS dimer interface, whereas the Arg binding sites are not (15, 17).

Conclusions and Perspectives—Our study establishes that nNOS differs from other mammalian NOSs regarding its dependence on N-terminal structure elements, and this helps to explain why nNOS is the only isoform that naturally exists as active N-terminally truncated splice variants. The biochemical data are entirely consistent with the N-terminal leader sequence and a downstream trio of core elements (N-terminal hook, the Zn^{2+} binding motif, and residues binding the H4B dihyroxypropyl side chain) representing two distinct subdomains within nNOS (18, 71). Genetic deletion of the leader subdomain permits a distinct cellular localization of native nNOS activity, whereas an additional genetic deletion of the core element subdomain permits distinct localization of an nNOS with significantly altered structural and catalytic properties that predispose it to generate reduced oxygen species along with NO. These features, together with distinct patterns of tissue expression, may enable nNOS to impact a wider range of physiological and pathophysiological processes including neurotransmission, skeletal muscle contraction, sexual functions, fluid homeostasis, addiction, atherosclerosis, and neurodegeneration (1–6). From an evolutionary point of view, it is intriguing that Δ349nNOSoxy (and presumably TnNOS and nNOSγ) display striking similarities with the bacterial NOS-like proteins with respect to having a significant dimer content and catalytic activity. This suggests that among the three NOS isoforms, only nNOS has maintained these characteristics in common with primitive NOS-like proteins and probably uses them to distinct advantage in higher organisms.

[2] J. Santolini and D. J. Stuehr, unpublished results.

REFERENCES

1. Dawson, V. L., and Dawson, T. M. (1998) *Prog. Brain Res.* **118,** 215–229
2. Harrison, D. G. (1997) *J. Clin. Invest.* **100,** 2153–2157
3. MacMicking, J., Xie, Q. W., and Nathan, C. (1997) *Annu. Rev. Immunol.* **15,** 323–350
4. Huang, Z., Huang, P. L., Panahian, N., Dalkara, T., Fishman, M. C., and Moskowitz, M. A. (1994) *Science* **265,** 1883–1885
5. Gross, S. S., and Wolin, M. S. (1995) *Annu. Rev. Physiol.* **57,** 737–769
6. Michel, T., and Feron, O. (1997) *J. Clin. Invest.* **100,** 2146–2152
7. Griffith, O. W., and Stuehr, D. J. (1995) *Annu. Rev. Physiol.* **57,** 707–736
8. Mayer, B., and Hemmens, B. (1997) *Trends Biochem. Sci.* **22,** 477–481
9. Dinerman, J. L., Lowenstein, C. J., and Snyder, S. H. (1993) *Circ. Res.* **73,** 217–222
10. Hemmens, B., and Mayer, B. (1998) *Methods Mol. Biol.* **100,** 1–32
11. Stuehr, D. J. (1999) *Biochim. Biophys. Acta* **1411,** 217–230
12. Baek, K. J., Thiel, B. A., Lucas, S., and Stuehr, D. J. (1993) *J. Biol. Chem.* **268,** 21120–21129
13. Klatt, P., Pfeiffer, S., List, B. M., Lehner, D., Glatter, O., Bachinger, H. P., Werner, E. R., Schmidt, K., and Mayer, B. (1996) *J. Biol. Chem.* **271,** 7336–7342
14. Rodriguez-Crespo, I., Gerber, N. C., and Ortiz de Montellano, P. R. (1996) *J. Biol. Chem.* **271,** 11462–11467
15. Crane, B. R., Arvai, A. S., Ghosh, D. K., Wu, C., Getzoff, E. D., Stuehr, D. J., and Tainer, J. A. (1998) *Science* **279,** 2121–2126
16. Ghosh, D. K., Wu, C., Pitters, E., Moloney, M., Werner, E. R., Mayer, B., and Stuehr, D. J. (1997) *Biochemistry* **36,** 10609–10619
17. Raman, C. S., Li, H., Martasek, P., Kral, V., Masters, B. S., and Poulos, T. L. (1998) *Cell* **95,** 939–950
18. Fischmann, T. O., Hruza, A., Niu, X. D., Fossetta, J. D., Lunn, C. A., Dolphin, E., Prongay, A. J., Reichert, P., Lundell, D. J., Narula, S. K., and Weber, P. C. (1999) *Nat. Struct. Biol.* **6,** 233–242
19. Bender, A. T., Nakatsuka, M., and Osawa, Y. (2000) *J. Biol. Chem.* **275,**

26018–26023
20. Ghosh, D. K., Abu-Soud, H. M., and Stuehr, D. J. (1996) *Biochemistry* **35,** 1444–1449
21. Siddhanta, U., Wu, C., Abu-Soud, H. M., Zhang, J., Ghosh, D. K., and Stuehr, D. J. (1996) *J. Biol. Chem.* **271,** 7309–7312
22. Panda, K., Ghosh, S., and Stuehr, D. J. (2001) *J. Biol. Chem.* **276,** 23349–23356
23. Sagami, I., Daff, S., and Shimizu, T. (2001) *J. Biol. Chem.* **276,** 30036–30042
24. Wang, Y., and Marsden, P. A. (1995) *Adv. Pharmacol.* **34,** 71–90
25. Wang, Y., Newton, D. C., and Marsden, P. A. (1999) *Crit. Rev. Neurobiol.* **13,** 21–43
26. Wang, Y., Newton, D. C., Robb, G. B., Kau, C. L., Miller, T. L., Cheung, A. H., Hall, A. V., VanDamme, S., Wilcox, J. N., and Marsden, P. A. (1999) *Proc. Natl. Acad. Sci. U. S. A.* **96,** 12150–12155
27. Brenman, J. E., Chao, D. S., Gee, S. H., McGee, A. W., Craven, S. E., Santillano, D. R., Wu, Z., Huang, F., Xia, H., Peters, M. F., Froehner, S. C., and Bredt, D. S. (1996) *Cell* **84,** 757–767
28. Lee, M. A., Cai, L., Hubner, N., Lee, Y. A., and Lindpaintner, K. (1997) *J. Clin. Invest.* **100,** 1507–1512
29. Ghosh, D. K., Crane, B. R., Ghosh, S., Wolan, D., Gachhui, R., Crooks, C., Presta, A., Tainer, J. A., Getzoff, E. D., and Stuehr, D. J. (1999) *EMBO J.* **18,** 6260–6270
30. Rodriguez-Crespo, I., Moenne-Loccoz, P., Loehr, T. M., and Ortiz de Montellano, P. R. (1997) *Biochemistry* **36,** 8530–8538
31. Wang, Y., Goligorsky, M. S., Lin, M., Wilcox, J. N., and Marsden, P. A. (1997) *J. Biol. Chem.* **272,** 11392–11401
32. Crane, B. R., Rosenfeld, R. J., Arvai, A. S., Ghosh, D. K., Ghosh, S., Tainer, J. A., Stuehr, D. J., and Getzoff, E. D. (1999) *EMBO J.* **18,** 6271–6281
33. Adak, S., Bilwes, A. M., Panda, K., Hosfield, D., Aulak, K. S., McDonald, J. F., Tainer, J. A., Getzoff, E. D., Crane, B. R., and Stuehr, D. J. (2002) *Proc. Natl. Acad. Sci. U. S. A.* **99,** 107–112
34. Adak, S., Aulak, K. S., and Stuehr, D. J. (2002) *J. Biol. Chem.* **277,** 16167–16171
35. Pant, K., Bilwes, A. M., Adak, S., Stuehr, D. J., and Crane, B. R. (2002) *Biochemistry* **41,** 11071–11079
36. Boyhan, A., Smith, D., Charles, I. G., Saqi, M., and Lowe, P. N. (1997) *Biochem. J.* **323,** 131–139
37. Adak, S., Santolini, J., Tikunova, S., Wang, Q., Johnson, J. D., and Stuehr, D. J. (2001) *J. Biol. Chem.* **276,** 1244–1252
38. Adak, S., Ghosh, S., Abu-Soud, H. M., and Stuehr, D. J. (1999) *J. Biol. Chem.* **274,** 22313–22320
39. Gachhui, R., Ghosh, D. K., Wu, C., Parkinson, J., Crane, B. R., and Stuehr, D. J. (1997) *Biochemistry* **36,** 5097–5103
40. Adak, S., Wang, Q., and Stuehr, D. J. (2000) *J. Biol. Chem.* **275,** 17434–17439
41. Boggs, S., Huang, L., and Stuehr, D. J. (2000) *Biochemistry* **39,** 2332–2339
42. Stankovich, M. T. (1980) *Anal. Biochem.* **109,** 295–308
43. Panda, K., Rosenfeld, R. J., Ghosh, S., Meade, A. L., Getzoff, E. D., and Stuehr, D. J. (2002) *J. Biol. Chem.* **277,** 31020–31030
44. Abu-Soud, H. M., Loftus, M., and Stuehr, D. J. (1995) *Biochemistry* **34,** 11167–11175
45. Abu-Soud, H. M., Wang, J., Rousseau, D. L., and Stuehr, D. J. (1999) *Biochemistry* **38,** 12446–12451
46. Ghosh, S., Wolan, D., Adak, S., Crane, B. R., Kwon, N. S., Tainer, J. A., Getzoff, E. D., and Stuehr, D. J. (1999) *J. Biol. Chem.* **274,** 24100–24112
47. Abu-Soud, H. M., Wu, C., Ghosh, D. K., and Stuehr, D. J. (1998) *Biochemistry* **37,** 3777–3786
48. Santolini, J., Meade, A. L., and Stuehr, D. J. (2001) *J. Biol. Chem.* **276,** 48887–48898
49. Abu-Soud, H. M., Presta, A., Mayer, B., and Stuehr, D. J. (1997) *Biochemistry* **36,** 10811–10816
50. Hemmens, B., Woschitz, S., Pitters, E., Klosch, B., Volker, C., Schmidt, K., and Mayer, B. (1998) *FEBS Lett.* **430,** 397–400
51. Christopherson, K. S., Hillier, B. J., Lim, W. A., and Bredt, D. S. (1999) *J. Biol. Chem.* **274,** 27467–27473
52. Jaffrey, S. R., Snowman, A. M., Eliasson, M. J., Cohen, N. A., and Snyder, S. H. (1998) *Neuron* **20,** 115–124
53. Ponting, C. P., Phillips, C., Davies, K. E., and Blake, D. J. (1997) *Bioessays* **19,** 469–479
54. Komeima, K., Hayashi, Y., Naito, Y., and Watanabe, Y. (2000) *J. Biol. Chem.* **275,** 28139–28143
55. Zanelli, S. A., Ashraf, Q. M., and Mishra, O. P. (2002) *Neuroscience* **112,** 869–877
56. Brenman, J. E., Chao, D. S., Xia, H., Aldape, K., and Bredt, D. S. (1995) *Cell* **82,** 743–752
57. Sagami, I., and Shimizu, T. (1998) *J. Biol. Chem.* **273,** 2105–2108
58. Hemmens, B., Goessler, W., Schmidt, K., and Mayer, B. (2000) *J. Biol. Chem.* **275,** 35786–35791
59. Scheele, J. S., Bruner, E., Zemojtel, T., Martasek, P., Roman, L. J., Masters, B. S., Sharma, V. S., and Magde, D. (2001) *J. Biol. Chem.* **276,** 4733–4736
60. Rodriguez-Crespo, I., Nishida, C. R., Knudsen, G. M., and de Montellano, P. R. (1999) *J. Biol. Chem.* **274,** 21617–21624
61. Gachhui, R., Abu-Soud, H. M., Ghosha, D. K., Presta, A., Blazing, M. A., Mayer, B., George, S. E., and Stuehr, D. J. (1998) *J. Biol. Chem.* **273,** 5451–5454
62. Santolini, J., Adak, S., Curran, C. M., and Stuehr, D. J. (2001) *J. Biol. Chem.* **276,** 1233–1243
63. Adak, S., and Stuehr, D. J. (2001) *J. Inorg. Biochem.* **83,** 301–308
64. Couture, M., Adak, S., Stuehr, D. J., and Rousseau, D. L. (2001) *J. Biol. Chem.* **276,** 38280–38288
65. Abu-Soud, H. M., Rousseau, D. L., and Stuehr, D. J. (1996) *J. Biol. Chem.* **271,** 32515–32518
66. Wang, Z. Q., Wei, C. C., Ghosh, S., Meade, A. L., Hemann, C., Hille, R., and Stuehr, D. J. (2001) *Biochemistry* **40,** 12819–12825
67. Martasek, P., Miller, R. T., Liu, Q., Roman, L. J., Salerno, J. C., Migita, C. T., Raman, C. S., Gross, S. S., Ikeda-Saito, M., and Masters, B. S. (1998) *J. Biol. Chem.* **273,** 34799–34805
68. Li, H., Raman, C. S., Glaser, C. B., Blasko, E., Young, T. A., Parkinson, J. F., Whitlow, M., and Poulos, T. L. (1999) *J. Biol. Chem.* **274,** 21276–21284
69. Bird, L. E., Ren, J., Zhang, J., Foxwell, N., Hawkins, A. R., Charles, I. G., and Stammers, D. K. (2002) *Structure* (*Cambr.*) **10,** 1687–1696
70. Chen, P. F., Tsai, A. L., Berka, V., and Wu, K. K. (1997) *J. Biol. Chem.* **272,** 6114–6118
71. Hillier, B. J., Christopherson, K. S., Prehoda, K. E., Bredt, D. S., and Lim, W. A. (1999) *Science* **284,** 812–815